Published in final edited form as:
Ultrasound Med Biol. 2009 May ; 35(5): 707. doi:10.1016/j.ultrasmedbio.2008.11.001.

ACOUSTIC RADIATION FORCE IMPULSE IMAGING FOR NONINVASIVE CHARACTERIZATION OF CAROTID ARTERY ATHEROSCLEROTIC PLAQUES: A FEASIBILITY STUDY

Jeremy J. Dahl[*], **Douglas M. Dumont**[*], **Jason D. Allen**[†], **Elizabeth M. Miller**[†], and **Gregg E. Trahey**[*]

[*] Department of Biomedical Engineering, Duke University, Durham, NC, USA

[†] Department of Medicine, Duke University Medical Center, Durham, NC, USA

Abstract

Atherosclerotic disease in the carotid artery is a risk factor for stroke. The susceptibility of atherosclerotic plaque to rupture, however, is challenging to determine by any imaging method. In this study, acoustic radiation force impulse (ARFI) imaging is applied to atherosclerotic disease in the carotid artery to determine the feasibility of using ARFI to noninvasively characterize carotid plaques. ARFI imaging is a useful method for characterizing the local mechanical properties of tissue and is complementary to B-mode imaging. ARFI imaging can readily distinguish between stiff and soft regions of tissue. High-resolution images of both homogeneous and heterogeneous plaques were observed. Homogeneous plaques were indistinguishable in stiffness from vascular tissue. However, they showed thicknesses much greater than normal vascular tissue. In heterogeneous plaques, large and small soft regions were observed, with the smallest observed soft region having a diameter of 0.5 mm. A stiff cap was observed covering the large soft tissue region, with the cap thickness ranging from 0.7–1.3 mm.

Keywords

Ultrasound; Ultrasonic imaging; Atherosclerosis; Carotid plaque; Radiation force; ARFI

INTRODUCTION

Stroke is the third leading causes of death in the United States, accounting for over 150,000 deaths in 2004. Ischemic stroke, or blockage of an artery to the brain, is the most common type of stroke and occurs in 87% of all strokes. Atherosclerotic disease is considered the primary cause of ischemic stroke. This process starts with initial vessel wall endothelial damage, monocyte infiltration, thickening of the intimal-medial arterial layers, formation of fatty streaks and eventually atherosclerotic plaques (Ross 1986). This narrowing of the vessel increases the chances of the formation of blood clots (thrombosis), which dislodge and move up to the brain (embolism). Interestingly, several studies have shown the morphology of the plaque itself may play a critical role in the incidence of ischemic neurologic events (AbuRahma et al. 1998; Tegos et al. 2001; Montauban van Swijndregt et al. 1999). This suggests plaque morphology is a potentially important factor in the selection of patients for carotid endarterectomy surgery (AbuRahma et al. 2002).

Address correspondence to: Jeremy J. Dahl, Duke University, Department of Biomedical Engineering, 136 Hudson Hall, Box 90281, Durham, NC 27708. jeremy.dahl@duke.edu.

Evidence in the literature suggests that ischemic stroke is associated less with calcified and fibrous plaques than with those containing softer tissue (Gomez 1990; Nandalur et al. 2005). The soft tissue in atherosclerotic plaque can consist of lipid pools, macrophages, foam cells, debris from intraplaque hemorrhage, as well as numerous other tissues due to the response of the immune system. The soft tissue is often surrounded by a fibrous cap, which is prone to rupture if the cap is thin. The definition of a vulnerable plaque remains somewhat unclear, however, as the cap thickness defining vulnerability varies in the literature from 65 μm (Tearney et al. 2003; Burke et al. 1997) to up to 700 μm (Ge et al. 1999; Fayad and Fuster 2001).

A recent trend in imaging atherosclerotic plaques has been to ascertain the vulnerability of a plaque to rupture via imaging characteristics or imaging the mechanical properties of the plaque. Plaque characterization by B-mode ultrasonography typically uses a subjective gray-scale classification, such as whether plaques are hypoechoic or hyperechoic, and homogeneous or heterogeneous (AbuRahma et al. 2002; Sabetai et al. 2000b; Tegos et al. 2001). Hypoechoic and heterogeneous plaques are often related to ipsilateral neurologic events (AbuRahma et al. 2002; Sabetai et al. 2000b). Unfortunately, the consistency between institutions and the reproducibility of the characterization of plaque morphology is relatively poor (Sabetai et al. 2000a).

Recently, intravascular optical coherence tomography (OCT) (Tearney et al. 2006) and intravascular ultrasound elastography (de Korte et al. 2002; Schaar et al. 2003) have been shown to identify atherosclerotic plaques in coronary arteries with good results. However, these techniques are relatively invasive in comparison to typical ultrasonic carotid examinations and OCT has difficulty in distinguishing vulnerable plaque characteristics in the carotid artery (Prabhudesai et al. 2006). Magnetic resonance imaging can be very sensitive to plaque composition (Lovett et al. 2005; Touzé et al. 2007; Saam et al. 2007; Kawahara et al. 2007) but it is very expensive for widespread use.

Ultrasonographic measures of carotid intimal-medial thickness (IMT) are associated with cardiovascular disease and have been shown to be an indicator for stroke (Lorenz et al. 2007; Leon Jr. et al. 2005; Chambless et al. 2000). Although this measurement is easily implemented and provides a general assessment of risk, the carotid IMT provides no information about the mechanical composition of plaques nor their vulnerability to rupture.

Radiation force-based imaging with ultrasound is an emerging field for imaging the mechanical properties of tissue. These methods include shear wave elasticity imaging (Sarvazyan et al. 1998), kinetic acoustic vitreoretinal examination (Walker et al. 2000), vibro-acoustography (Fatemi and Greenleaf 1999), supersonic shear imaging (Bercoff et al. 2004) and acoustic radiation force impulse (ARFI) imaging (Nightingale et al. 2001, 2002).

ARFI imaging is a radiation force-based imaging method that uses commercially available ultrasound scanners to generate short duration acoustic radiation forces. These impulses generate localized displacements in tissue of approximately 1–10 μm. The response of the tissue to the radiation force is observed using conventional B-mode imaging pulses. ARFI imaging has been employed to observe the mechanical properties of excised vessels (Trahey et al. 2004) and *in vivo* popliteal arteries (Dumont et al. 2006).

In our previous studies of an excised human vessel containing an atherosclerotic plaque (Trahey et al. 2004), we observed with ARFI imaging a soft region surrounded by stiffer tissue in the wall of a vessel containing a large atherosclerotic plaque. Pathology examination of the plaque revealed a lipid core surrounded by fibrous tissue at this location. The lipid core corresponded well with the region in the ARFI image depicted as high displacement, a characteristic of soft tissue. Regions of the vessel portrayed as very stiff were shown to contain calcifications in the

histologic samples. Healthy portions of the vessel were shown to be stiffer than the soft plaque region, but more compliant than the calcified region.

The goal of this study was to determine the feasibility of using ARFI imaging to generate high resolution images of carotid plaques *in vivo*. We employ ARFI imaging to noninvasively characterize atherosclerotic plaque in the carotid artery of several volunteers.

METHODS

Using the Framingham Coronary Heart Disease Prediction Algorithm (Wilson et al. 1998) we recruited and classified volunteers as high (n = 14) or low (n = 9) risk for cardiovascular disease. Classification under this algorithm included risk factors such as blood pressure, cholesterol, age, diabetes and smoking. All volunteers were recruited under an Institutional Review Board approved protocol (registry number 7874) and informed consent was obtained for each volunteer prior to imaging. All B-mode and ARFI scans of the carotid arteries were performed at the Frederick R. Cobb Noninvasive Vascular Research Laboratory at the Duke Center for Living Campus.

The volunteers were not screened for plaques in the carotid vasculature, so the incidence of a plaque and degree of stenosis in the volunteers were unknown prior to imaging. The volunteers were not scheduled for endarterectomies or other types of intervention and, therefore, no histologic samples were available.

For each participant, short B-mode clips (5 s) of the common carotid artery, its bifurcation and the internal carotid artery were recorded in order to assess the IMT. Using the Carotid Analyzer for Research software (Medical Imaging Applications, Coralville, IA, USA), the IMT of each segment of artery was measured and given a percentile score using the Atherosclerotic Risk in Communities (ARIC) database (Howard et al. 1993).

ARFI imaging was implemented on a modified Siemens Antares™ scanner and a VF10-5 array (Siemens Medical Solutions USA, Inc., Issaquah, WA, USA) to obtain displacement images of the carotid vasculature. In an ARFI imaging sequence, a reference A-line is acquired at one location, which is then followed with an extended duration pulse at the same location. This extended duration pulse is called a pushing pulse because it provides the radiation force and displaces the tissue a small amount (1–10 μm). The pushing pulses used for ARFI imaging of the carotid artery were 24 to 59 μs in duration (at 5.7 MHz), depending on the depths of the vessel walls. For each location a pushing pulse was focused at both the proximal and distal walls. The depth of the proximal and distal walls varied from patient to patient, ranging from 0.8 to 1.6 cm for the proximal wall, and 1.6 to 2.4 cm for the distal wall.

Following the pushing pulse, a series of A-lines were acquired at the same location. These lines are used to track the displacements caused by the pushing pulse using cross-correlation or phase-shift estimation techniques and are, therefore, referred to as tracking lines. The response of the proximal and distal walls to the pushing pulses was observed for approximately 6.4 ms with a temporal sampling rate of 9.4 kHz. The tracking pulses used the default pulse from the scanner and a center frequency of 8 MHz. In-phase and quadrature (I/Q) data were captured using the Axius Direct™ Ultrasound Research Interface (URI) (Brunke et al. 2007), a data capture tool available on the Antares scanner.

The localized displacements were tracked using Loupas' two-dimensional autocorrelation technique (Loupas et al. 1995; Pinton et al. 2006) with a 0.1 mm kernel size. Eighty lateral locations were observed using a 4:1 parallel tracking method (Dahl et al. 2007) to minimize the amount of acoustic exposure and reduce transducer and tissue heating. This reduced the total number of pushes necessary to generate each ARFI image to 40 (20 each for the proximal

and distal walls). For each ARFI image acquired, a B-mode image was acquired immediately preceding the ARFI image.

For each plaque observed in a volunteer, between two and four ARFI imaging data sets were acquired to assess repeatability of the image. A pause of a few seconds was allowed between each acquired ARFI image in order to confirm data acquisition. In the displayed images, only a single data set was used to generate the image. Displacement images of the proximal and distal walls were generated 0.43 ms after application of the radiation force. The displacement images from the proximal and distal walls were then blended to generate the final ARFI image.

A mask was applied to the ARFI images in order to eliminate the displacement noise measured in the lumina of the blood vessels. The continuous movement of the blood appears to the displacement estimator as high spatially-variant displacements and makes visualizing the image difficult. To implement a mask of the blood, the temporal variance of the ARFI displacements was computed over the last 2.1 ms of tracking. In the regions of the image where the variance was greater than 0.7 μm^2, the color was set to black. Although this mask removes the great majority of the noise and displays a reasonable visualization of the vessel lumen, some displacement noise was still visible in the lumen area. This remaining noise is removed by manually setting the color of these areas to black to produce a more aesthetically pleasing image.

ARFI images have previously been shown to display the complete vessel wall, including the adventitial, intimal and medial layers (Trahey et al. 2004). B-mode ultrasonography typically displays the intimal and medial layers well, but identification of the adventitial layer can be difficult. The thickness of the vessel walls were measured in the ARFI images and compared with the conventional IMT measurements. The wall thickness was measured as the distance from the sharp boundary between regions of high tissue displacement and low tissue displacement (the expected tissue/vessel interface) to the boundary between low displacement/variance and high spatial/temporal variance (the expected vessel/lumen interface). A Student's *t* test was used to compare the high and low risk groups and the ARFI-derived and IMT measurements. The *p* value was computed for each comparison.

Because of the long pushing pulses used in ARFI imaging, the heating associated with these pulses can be significant. Therefore, the imaging sequences must be designed to minimize heating of both the tissue and transducer surface. A simulation of tissue heating was performed using the heating model described by Palmeri and Nightingale (2004), which has been shown to be an accurate model for tissue heating from ARFI imaging (Palmeri et al. 2004). The maximum heat predicted by this model is 0.04°C for one image, given a tissue absorption of 0.5 dB/cm•MHz, thermal conductivity of 6.0 mW/cm/°C, and a specific heat of 4.2 J/cm^3•°C. The thermal material properties used for the simulation are associated with generic soft tissue as specified in the National Council on Radiation Protection and Measurements (NCRP) Report #113 (NCRP 1992). The temperature increase of 0.04°C is well below the Food and Drug Administration (FDA) limit on temperature increase (Food and Drug Administration, Center for Devices and Radiological Health 1997).

RESULTS

Tables 1 (high risk) and 2 (low risk) show the intimal-medial thickness of the common carotid artery measured from the B-mode images, its corresponding ARIC Study percentile and the wall thickness (adventitial layer plus IMT) measured from the ARFI images. The ARIC percentile relates the distal wall IMT of the individual to the distal wall IMT of the larger community (Howard et al. 1993), and is adjusted for age, gender and race. This percentile has been shown to be correlated with the risk for stroke (Chambless et al. 2000).

The wall thickness values for the high risk group were significantly larger than the low risk subjects for both the proximal and distal walls ($p = 0.003$ and $p = 0.005$, respectively). In addition, the IMTs for the high risk group were significantly larger than the low risk group as anticipated ($p = 0.007$ and $p = 0.008$ for the proximal and distal IMT, respectively). The ARIC percentiles were also statistically significant between the high and low risk groups ($p = 0.01$). Further analysis revealed that the adventitia thickness (arterial wall thickness - IMT) was not different between groups for the proximal or distal walls ($p = 0.97$ and $p = 0.14$, respectively). The average adventitial thickness in the proximal wall was 0.7 ± 0.2 and 0.7 ± 0.3 mm for the low and high risk groups, respectively. The average adventitial thickness in the distal wall was 0.6 ± 0.1 mm in the low risk group and 0.7 ± 0.4 mm in the high risk group.

Figures 1 to 6 show matched B-mode and ARFI images of healthy and diseased carotid arteries. The field-of-view of the ARFI image is matched to the region in the corresponding B-mode image that is bounded by white lines. Common anatomical structures are labeled in each image and include the common carotid artery (CCA), internal carotid artery (ICA), proximal wall (PW), distal wall (DW) and jugular vein (JV). Because the B-mode and ARFI images are acquired on consecutive heartbeats, there may be some mismatch in position between the two images.

Figure 1 displays the matched B-mode and ARFI images for a healthy common carotid artery in a 46-y-old female. For a normal, healthy vessel, uniform displacement is observed across the entire vessel length (approximately 4 μm in the distal wall and 2 μm in the proximal wall). Differences in mean displacement in the proximal and distal walls occur due to focal and absorption effects of the radiation force and the relative position of the wall to the region of excitation. The key information, therefore, is the relative displacement in the regions local to each vessel wall.

The IMT measurements for the proximal and distal walls were 0.48 mm and 0.51 mm, respectively, which are consistent with healthy carotid tissue. Note that the adventitial layer is not easily visible in B-mode scanning. The adventitial tissue is visible in the ARFI image, but is not distinguishable from the intimal and medial layers.

Figure 2 displays the matched B-mode and ARFI images for a common carotid artery in a 67-y-old male with thickening of the intimal-medial layer due to atherosclerotic disease. The images in Fig. 2 are representative of a number of volunteers we observed in our study. Thickening is apparent in both the B-mode and ARFI images on the proximal wall in the right portion of the images but the atherosclerosis is indistinguishable from normal vasculature in terms of its stiffness. The IMT measurements for the proximal and distal walls were 1.21 mm and 1.07 mm, respectively. Carotid IMT measurements of this size are consistent with diseased tissue.

Figures 3 and 4 display an example of a stiff, possibly fibrous, plaque in the common carotid artery of a 49-y-old male. The B-mode image in Fig. 3 shows a cross-sectional view of the carotid artery with the jugular vein located to the upper left of the carotid artery. The plaque is partially visible in the B-mode image, located on the right side of the artery and occludes approximately 40% of the vessel cross-section. In the ARFI image, the plaque is visible in the right portion of the vessel and has high contrast with the surrounding soft tissue. In this image, the displacements produced in the plaque are uniform throughout.

Figure 4 displays the longitudinal view of the plaque. The B-mode image indicates a plaque on the far wall of the common carotid artery. As shown in Fig. 3, the plaque appears to wrap around a significant portion of the artery and is, therefore, visible on the near wall of the common carotid artery. The view of the plaque in the longitudinal axis shows the plaque to be homogeneously stiff throughout.

Figure 5 shows an example of an apparently heterogeneous plaque containing a soft region surrounded by a stiff cap in the carotid bifurcation of a 55-y-old female volunteer. The plaque is located near the bifurcation of the carotid artery and appears to wrap around the artery such that it is visible on both the proximal and distal walls.

The soft region of the plaque is visible on the distal wall as the oval shaped region extending from 23 to 25 mm depth and −2 to 4 mm laterally in the ARFI image. The soft region is surrounded by a significantly stiffer region. The displacement of the soft region ranges from 5 to 8 μm, compared with 2 μm in the surrounding stiffer tissue. The surrounding tissue is approximately 1.3 mm thick between the soft region and the vessel lumen, except on the left side, where the thickness of the cap decreases to approximately 0.7 mm. At 0.7 mm, the stiff cap is at the upper limit of the range indicating vulnerability (Ge et al. 1999). Ge et al. (1999) also noted that a lipid core with area greater than 1 mm^2 or a core to plaque ratio greater than 20% also correlated well with rupture. The soft region in this plaque meets Ge's definition of a vulnerable plaque, assuming that this region is a lipid core. This soft region was only partially visible in the second ARFI image acquired of this plaque, however, there was a significant amount of motion between acquisitions that may have changed the imaging plane.

Figure 6 displays an example of a stiff plaque containing mild heterogeneity in the carotid bifurcation of an 83-y-old male. The B-mode image indicates a large plaque extending across the distal wall of the carotid bifurcation. The main portion of the plaque is situated at the bifurcation with a less visible secondary lump located at approximately −10 mm laterally. A significant amount of calcification is present in the B-mode image as indicated by the shadowing distal to the plaque.

This plaque contains two small regions of tissue that are soft relative to the surrounding plaque. The first soft tissue region is 0.5 mm in size and is located in the center of the large plaque at the bifurcation of the carotid artery. This region displaces approximately twice that of the surrounding plaque. Observation of the region of displacement through time in Fig. 7 reveals that this region initially displaced approximately three times greater than the surrounding plaque and reached its peak displacement much earlier than the time step for which this image was created. In addition, this soft region recovered to its original position much slower than the surrounding plaque. The second region of soft tissue appears in the smaller protruding plaque in the internal carotid artery. This soft tissue region has characteristics similar to the soft tissue in the larger plaque. These soft regions were visible in three ARFI images taken of this plaque.

The presence of calcification in this plaque is consistent with the low displacement at the calcification site. Below the calcification (at 25–28 mm depth), displacements of approximately 1 μm are obtained whereas locations lateral to this show relatively high displacement. This is due to severe attenuation of the radiation force from the calcification. The large displacements observed in the proximal wall of the ICA are an artifact most likely caused by reverberation of the ultrasound pulse in the soft tissue layers proximal to the jugular vein. As the soft tissue in the region causing reverberations is displaced, the reverberant echoes appear to displace as well. These reverberation artifacts are not a major concern for misjudgment of tissue structures because they are fairly apparent and can be easily identified in B-mode images (as in this case).

DISCUSSION

Tables 1 and 2 indicate the ARIC percentile rank of common carotid IMT thickness for each of the volunteer subjects. This score has been shown to be correlated with the risk for stroke (Lorenz et al. 2007;Leon Jr. et al. 2005;Chambless et al. 2000). These metrics do not indicate, however, whether a particular plaque may be prone to rupture. Knowledge of the mechanical

makeup of plaques may allow clinicians to better differentiate patients that are at higher risk for ischemic neurologic events. This may aid in the selection of candidates for carotid endarterectomy surgery. In addition, the ARIC percentiles only account for intimal-medial thickening of the distal wall. Atherosclerosis can also occur on the proximal wall, and therefore may not accurately reflect the true risk of the patient.

Histologic confirmation of the plaques observed in Figs. 3 to 6 was unavailable, so definitive makeup of these plaques were unknown. However, the structures and mechanical properties in the ARFI images observed in this study are consistent with our excised vessel study (Trahey et al. 2004) for which histologic confirmation has been performed. In excised vessels, fibrous plaque and calcified regions were associated with very low displacements relative to the surrounding tissue, whereas relatively large displacements were observed in soft, lipid-filled regions.

The important information in the ARFI images is the relative, and not absolute, displacements incurred in each tissue. This is because the force used to generate the displacements can vary from person to person and tissue to tissue depending on other factors including differences in overlying tissue, attenuation and the position of the vessel. Because radiation force was applied to both the proximal and distal walls in Figs. 1 to 6, only the displacements in the adjacent tissues should be compared and not the displacements between the two walls.

There is a possibility that two significantly different tissue types can be displaced equally by the same applied force if one tissue is softer and weakly absorbs ultrasound waves and the other is stiffer and greatly absorbs ultrasound waves. Given the reported values of elastic modulus and attenuation of plaque tissues, however, it seems that this scenario is unlikely. Lipid-filled regions are reported to be 1/100 the modulus of normal arterial tissue (Keeny and Richardson 1987) and fibrous and calcified plaque have moduli orders of magnitude greater than normal tissue (Baldewsing et al. 2004; Cheng et al. 1994; Lee et al. 1994). Fatty and calcified regions of atherosclerotic plaque are reported to have greater attenuation than normal tissue, although the reported values of each vary widely (Greenleaf et al. 1974; Landini et al. 1985). Fibrous tissue was shown to have similar attenuation as normal tissue (Greenleaf et al. 1974).

In most instances, it was found that ARFI imaging is incapable of detecting the difference in stiffness between hard plaque and vascular tissue. Both tissues are very stiff and displace no more than 2 to 4 μm at the forces applied in this setup. In addition, ARFI imaging is incapable of identifying the different types of soft tissue present in plaques (Figs. 5 and 6). These tasks are not crucial to determining plaque vulnerability, however, because vulnerability is largely defined by the plaque morphology and its composition. The vast majority of plaques are composed of three main tissues, which are dense fibrous tissue, calcifications and lipid-rich/necrotic cores (Gomez 1990;Fayad and Fuster 2001;Saam et al. 2005). Alternatively, MRI does have the advantage of distinguishing different soft tissue types with good sensitivity and specificity as well as differentiating dense fibrous tissue (Saam et al. 2007) but the cost of using MRI for such screening may be prohibitive.

ARFI imaging is capable of detecting soft regions as small as 0.5 mm in diameter (see Fig. 6). Several reasons support this region being identified as soft rather than a noise artifact. First, the axial resolution is dependent on the pulse length (or transducer bandwidth) and the kernel size (Jensen 1996), with the lower limit of resolution being half the pulse length. In this case, we chose a kernel length of 0.1 mm, which is approximately equal to one-half the pulse length. The lateral resolution of the ARFI images is similar to that of B-mode imaging, and is dependent on the beam width and the lateral sample spacing. The lateral resolution in these images is 0.3 mm. Second, the error in the displacement calculation typically seen in ARFI images is on the

order of a few tenths of microns. Empirical measurements of the jitter from a phantom with a similar SNR (estimated to be 20 dB in the shadowed region under the plaque in Fig. 6), indicated that the jitter, or the standard deviation of the error in the estimates, is approximately 1.2 μm. Third, the reproducibility of ARFI images is good. The temporal stability of the soft tissue regions was confirmed with multiple ARFI images of the plaques taken several seconds apart from each other (and with small shifts in spatial location). In Fig. 6, the soft regions were visible in three of the four ARFI images. Lastly, the soft regions recover to the noise floor (1.2 μm) in a significantly longer time than the hard region (see Fig. 7), which is a behavior of different tissue types rather than jitter noise. Due to the size of these soft regions, they cannot be modeled as linear, isotropic, elastic tissue. However, the recovery of this tissue due to radiation force is consistent with the response expected from linear, isotropic, elastic tissue (Palmeri et al. 2006).

The wall thickness measurements derived by ARFI imaging are consistently larger than IMT measurements but may yield no additional information to current IMT measurements. However, they may provide easier and more consistent measurements in difficult-to-image patients. Carotid IMT measurements can only be applied to segments where the IMT layer is visible in the B-mode image. This is not typically achieved over the entire vessel and is often more difficult to achieve in the proximal wall than in the distal wall. ARFI imaging may be able to aid B-mode IMT measurements in this regard. For example, the ARFI image shown in Fig. 5 shows good visualization of the proximal wall where the IMT layer is not well resolved in the B-mode image. It is unlikely that ARFI imaging will be a replacement for B-mode IMT measurements because ARFI images do not always yield good visualization of the vessel walls. For example, in Fig. 5 the distal wall of the vessel is not well resolved for most of the segment. Visualization problems can occur when the radiation force reaching the vessel wall is weak, such as when absorption is high or if the vessel wall lies deeper than the focal point of the radiation force. Improved instrumentation and transducers may overcome these limitations.

CONCLUSIONS

The feasibility of imaging atherosclerotic plaques in the carotid artery with acoustic radiation force was demonstrated. High-resolution images of the mechanical properties of homogeneous and heterogeneous plaques were observed. Although no histologic samples could be obtained from the plaques in this study, the results were consistent with the displacements observed in excised vessels containing stiff, calcified and fibrous plaques and soft, lipid-filled regions. ARFI imaging was shown to be an effective, non-invasive technique for observing the mechanical makeup of carotid plaques.

Acknowledgments

This work is supported by NIH grants R01-HL075485 and R01-CA1 14093. The authors wish to thank the Ultrasound Division at Siemens Medical Solutions USA, Inc. for their in-kind and technical support.

References

AbuRahma AF, Kyer RD, Robinson PA, Hannay RS. The correlation of ultrasonic carotid plaque morphology and carotid plaque hemorrhage: Clinical implications. Surgery 1998;24:721–728. [PubMed: 9780994]

AbuRahma AF, Thiele SP, Wulu JT. Prospective controlled study of the natural history of asymptomatic 60% to 69% carotid stenosis according to ultrasonic plaque morphology. J Vasc Surg 2002;36:437–442. [PubMed: 12218962]

Baldewsing RA, de Korte CL, Schaar JA, Mastik F, van der Steen AFW. A finite element model for performing intravascular ultrasound elastography of human atherosclerotic coronary arteries. Ultrasound Med Biol 2004;30:803–813. [PubMed: 15219960]

Bercoff J, Tanter M, Fink M. Supersonic shear imaging: A new technique for soft tissue elasticity mapping. IEEE Trans Ultrason Ferroelectr Freq Control 2004;51:396–409. [PubMed: 15139541]

Brunke SS, Insana MF, Dahl JJ, Hansen C, Ashfaq M, Ermert H. An ultrasound research interface for a clinical system. IEEE Trans Ultrason Ferroelectr Freq Control 2007;54:198–210. [PubMed: 17225815]

Burke AP, Farb A, Malcom GT, Liang Y-H, Smialek J, Virmani R. Coronary risk factors and plaque morphology in men with coronary disease who died suddenly. N Engl J Med 1997;336:1276–1282. [PubMed: 9113930]

Chambless LE, Folsom AR, Clegg LX, Sharrett AR, Shahar E, Nieto FJ, Rosamond WD, Evans G. Carotid wall thickness is predictive of incident clinical stroke. The Atherosclerosis Risk in Communities (ARIC) Study. Am J Epidemiol 2000;151:478–487. [PubMed: 10707916]

Cheng GC, Loree HM, Kamm RD, Fishbein MC, Lee RT. Distribution of circumferential stress in ruptured and stable atherosclerotic lesions: A structural analysis with histopathologic correlation. Circulation 1994;87:1179–1187. [PubMed: 8462145]

Dahl JJ, Pinton GF, Palmeri ML, Agrawal V, Nightingale KR, Trahey GE. A parallel tracking method for acoustic radiation force impulse imaging. IEEE Trans Ultrason Ferroelectr Freq Control 2007;54:301–312. [PubMed: 17328327]

de Korte CL, Sierevogel MJ, Mastik F, Strijder C, Schaar J, Velema E, Pasterkamp G, Serruys PW, van der Steen AFW. Identification of atherosclerotic plaque components with intravascular ultrasound elastography in vivo: A Yucatan pig study. Circulation 2002;105:1627–1630. [PubMed: 11940537]

Dumont D, Miller E, Allen JD, Moyer C, Hsu S, Trahey GE. Peripheral vascular ARFI imaging: Phantom and clinical results. Proc IEEE Ultrason Symp 2006;1:605–608.

Fatemi M, Greenleaf JF. Vibro-acoustography: An imaging modality based on ultrasound-stimulated acoustic emission. Proc Natl Acad Sci USA 1999;96:6603–6608. [PubMed: 10359758]

Fayad ZA, Fuster V. Clinical imaging of the high risk or vulnerable atherosclerotic plaque. Circulation Res 2001;89:305–316. [PubMed: 11509446]

Food and Drug Administration - Center for Devices and Radiologic Health. Technical Report. US Department of Health and Human Services; 1997. Information for manufacturers seeking marketing clearance of diagnostic ultrasound systems and transducers. www.fda.gov/cdrh/ode/ulstran.pdf

Ge J, Chirillo F, Schwedtmann J, Gorge G, Haude M, Baumgart D, Shah V, von Birgelen C, Sack S, Boudoulas H, Erbel R. Screening of ruptured plaques in patients with coronary artery disease by intravascular ultrasound. Heart 1999;81:621–627. [PubMed: 10336922]

Gomez CR. Carotid plaque morphology and risk for stroke. Stroke 1990;21:148–151. [PubMed: 2405546]

Greenleaf JF, Duck FA, Samayoa WF, Johnson SA. Ultrasonic data acquisition and processing system for atherosclerotic tissue characterization. Proc IEEE Ultrason Symp 1974:738–743.

Howard G, Sharrett AR, Heiss G, Evans GW, Chambless LE, Riley WA, Burke GL. Carotid artery intimal-medial thickness distribution in general populations as evaluated by B-mode ultrasound. ARIC Investigators Stroke 1993;24:1297–1304.

Jensen, JA. Estimation of blood velocities using ultrasound: A signal processing approach. Cambridge, Great Britain: Cambridge University Press; 1996.

Kawahara I, Morikawa M, Honda M, Kitagawa N, Tsutsumi K, Nagata I, Hayashi T, Koji T. High-resolution magnetic resonance imaging using gadolinium-based contrast agent for atherosclerotic carotid plaque. Surg Neurol 2007;68:60–66. [PubMed: 17586225]

Keeny, SM.; Richardson, PD. Stress analysis of atherosclerotic arteries. Eng Med Biol Soc; Proceedings of the IEEE Ninth Annual Conference; 1987. p. 1484-1485.

Landini L, Picano E, Sarnelli R. Attenuation measurements in atherosclerotic tissues: Problems with phase-cancellation artefacts. Med Biol Eng Comput 1985;23:220–223. [PubMed: 3894819]

Lee RT, Loree HM, Fishbein MC. High stress regions in saphenous vein bypass graft atherosclerotic lesions. J Am Coll Cardiol 1994;24:1639–1644. [PubMed: 7963109]

Leon, LR., Jr; Brewster, LP.; Labropoulos, N. Noninvasive Screening and Utility of Carotid Intima-Media Thickness. 2. Vol. chap 14. Philadelphia, PA: Saunders Elsevier; 2005. Vascular Diagnosis; p. 157-173.

Lorenz MW, Markus HS, Bots ML, Rosvall M, Sitzer M. Prediction of clinical cardiovascular events with carotid intima-media thickness: A systematic review and meta-analysis. Circulation 2007;115:459–467. [PubMed: 17242284]

Loupas T, Peterson R, Gill R. Experimental evaluation of velocity and power estimation for ultrasound blood flow imaging, by means of a two-dimensional autocorrelation approach. IEEE Trans Ultrason Ferroelectr Freq Control 1995;42:689–699.

Lovett JK, Redgrave JNE, Rothwell PM. A critical appraisal of the performance, reporting, and interpretation of studies comparing carotid plaque imaging with histology. Stroke 2005;36:1085–1091.

Montauban van Swijndregt AD, Elbers HRJ, Moll FL, de Letter J, Ackerstaff RGA. Cerebral ischemic disease and morphometric analyses of carotid plaques. Ann Vasc Surg 1999;13:468–474. [PubMed: 10466989]

Nandalur KR, Baskurt E, Hagspiel KD, Phillips CD, Kramer CM. Calcified carotid atherosclerotic plaque is associated less with ischemic symptoms than is noncalcified plaque on MDCT. Am J Roentgenol 2005;184:295–298. [PubMed: 15615991]

National Council on Radiation Protection and Measurements, Criteria Based on Thermal Mechanisms. Bethesda, MD 20814: NCRP Publications; 1992. Report No. 113: Exposure Criteria for Medical Diagnostic Ultrasound: I.

Nightingale KR, Palmeri ML, Nightingale RW, Trahey GE. On the feasibility of remote palpation using acoustic radiation force. J Acoust Soc Am 2001;110:625–634. [PubMed: 11508987]

Nightingale KR, Soo MS, Nightingale RW, Trahey GE. Acoustic Radiation Force Impulse imaging: In vivo demonstration of clinical feasibility. Ultrasound Med Biol 2002;28:227–235. [PubMed: 11937286]

Palmeri ML, Frinkley KD, Nightingale KR. Experimental studies of the thermal effects associated with radiation force imaging of soft tissue. Ultrasonic Imaging 2004;26:100–114. [PubMed: 15344414]

Palmeri ML, McAleavey SA, Fong K, Trahey GE, Nightingale KR. Dynamic mechanical response of elastic spherical inclusions to impulsive acoustic radiation force excitation. IEEE Trans Ultrason Ferroelectr Freq Control 2006;53:2065–2079. [PubMed: 17091842]

Palmeri ML, Nightingale KR. On the thermal effects associated with radiation force imaging of soft tissue. IEEE Trans Ultrason Ferroelectr Freq Control 2004;51:551–565. [PubMed: 15217233]

Pinton GF, Dahl JJ, Trahey GE. Rapid tracking of small displacements with ultrasound. IEEE Trans Ultrason Ferroelectr Freq Control 2006;53:1103–1117. [PubMed: 16846143]

Prabhudesai V, Phelan C, Yang Y, Wang RK, Cowling MG. The potential role of optical coherence tomography in the evaluation of vulnerable carotid atheromatous plaques: A pilot study. Cardiovasc Intervent Radiol 2006;29:1039–1045. [PubMed: 16967226]

Ross R. The pathogenesis of atherosclerosis—An update. N Engl J Med 1986;314:488–500. [PubMed: 3511384]

Saam T, Ferguson MS, Yarnykh VL, Takaya N, Xu D, Polissar NL, Hatsukami TS, Yuan C. Quantitative evaluation of carotid plaque composition by in vivo MRI. Arterioscler Thromb Vasc Biol 2005;25:234–239. [PubMed: 15528475]

Saam T, Hatsukami TS, Takaya N, Chu B, Underhill H, Kerwin WS, Cai J, Ferguson MS, Yuan C. The vulnerable, or high risk, atherosclerotic plaque: Noninvasive MR imaging for characterization and assessment. Radiology 2007;244:64–77. [PubMed: 17581895]

Sabetai MM, Tegos TJ, Nicolaides AN, Dhanjil S, Pare GJ, Stevens JM. Reproducibility of computer-quantified carotid plaque echogenicity. Can we overcome the subjectivity? 2000a;31:2189–2196.

Sabetai MM, Tegos TJ, Nicolaides AN, El-Atrozy TS, Dhanjil S, Griffin M, Belcaro G, Geroulakos G. Hemispheric symptoms and carotid plaque echomorphology. J Vasc Surg 2000b;31:39–49. [PubMed: 10642707]

Sarvazyan AP, Rudenko OV, Swanson SD, Fowlkes JB, Emelianov SY. Shear wave elasticity imaging: A new ultrasonic technology of medical diagnostics. Ultrasound Med Biol 1998;24:1419–1435. [PubMed: 10385964]

Schaar JA, de Korte CL, Mastik F, Strijder C, Pasterkamp G, Boersma E, Serruys PW, van der Steen AFW. Characterizing vulnerable plaque features with intravascular elastography. Circulation 2003;108:2636–2641. [PubMed: 14581406]

Tearney GJ, Jang I-K, Bouma BE. Optical coherence tomography for imaging the vulnerable plaque. J Biomed Opt 2006;11:021002. [PubMed: 16674177]

Tearney GJ, Yabushita H, Houser SL, Aretz HT, Jang I-K, Schlendorf KH, Kauffman CR, Shishkov M, Halpern EF, Bouma BE. Quantification of macrophage content in atherosclerotic plaques by optical coherence tomography. Circulation 2003;107:113–119. [PubMed: 12515752]

Tegos TJ, Stavropoulos P, Sabetai MM, Khodabakhsh P, Sassano A, Nicolaides AN. Determinants of carotid plaque instability: Echoicity versus heterogeneity. Eur J Vasc Endovasc Surg 2001;22:22–30. [PubMed: 11461098]

Touzé E, Toussaint J-F, Coste J, Schmitt E, Bonneville F, Vandermarcq P, Gauvrit J-Y, Douvrin F, Meder J-F, Mas J-L, Oppenheim C. Reproducibility of high- resolution MRI for the identification and the quantification of carotid atherosclerotic plaque components: Consequences for prognosis studies and therapeutic trials. Stroke 2007;38:1812–1819. [PubMed: 17463311]

Trahey GE, Palmeri ML, Bently RC, Nightingale KR. Acoustic radiation force impulse imaging of the mechanical properties of arteries: In vivo and ex vivo results. Ultrasound Med Biol 2004;30:1163–1171. [PubMed: 15550320]

Walker WF, Fernandez FJ, Negron LA. A method of imaging visco-elastic parameters with acoustic radiation force. Physics Med Biol 2000;45:1437–1447.

Wilson PWF, D'Agostino RB, Levy D, Belanger AM, Silbershatz H, Kannel WB. Prediction of coronary heart disease using risk factor categories. Circulation 1998;97:1837–1847. [PubMed: 9603539]

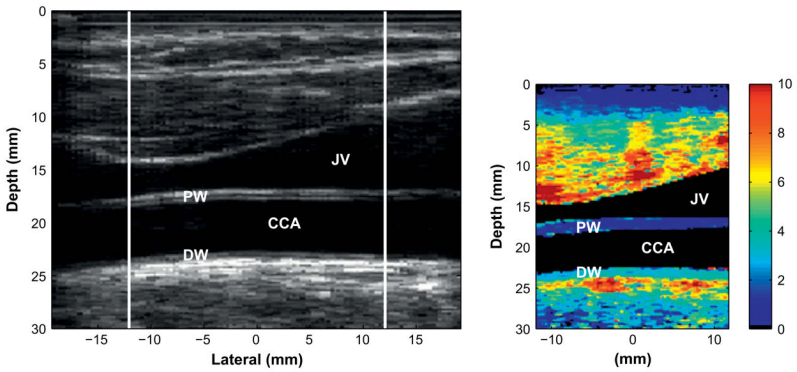

Fig. 1.

Matched B-mode (left) and corresponding acoustic radiation force impulse (ARFI) image (right) of a healthy carotid artery in a 46-y-old female. The color bar on the right indicates the amount of displacement in microns. The display is limited to 10 μm of displacement. Displacements are approximately 2 μm in the proximal wall of the vessel and 4 μm in the distal wall. Differences in wall displacement are expected due to differing applications of radiation force at the two walls.

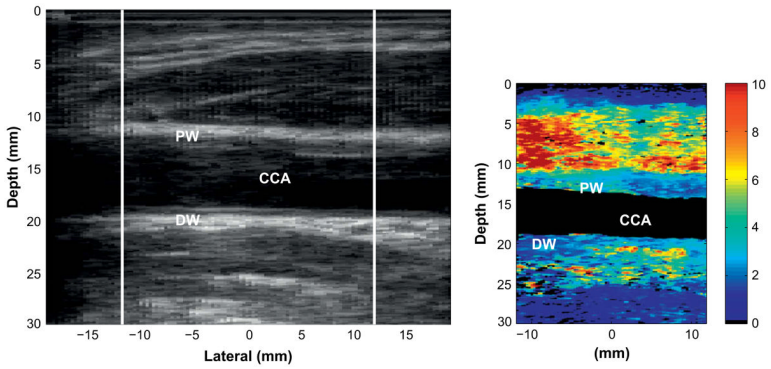

Fig. 2.

Matched B-mode (left) and corresponding ARFI image (right) of the common carotid artery of a 67-y-old male with thickening pertaining to atherosclerotic disease.

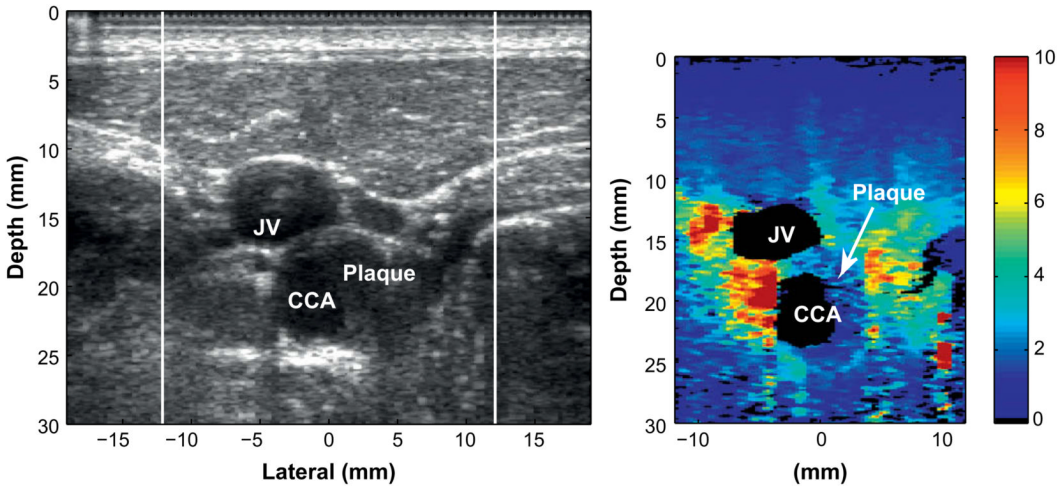

Fig. 3.

Matched B-mode (left) and corresponding ARFI image (right) of a stiff plaque in a 49-y-old male patient. The plaque is visible on the right side of the carotid artery with high contrast relative to the surrounding soft tissue.

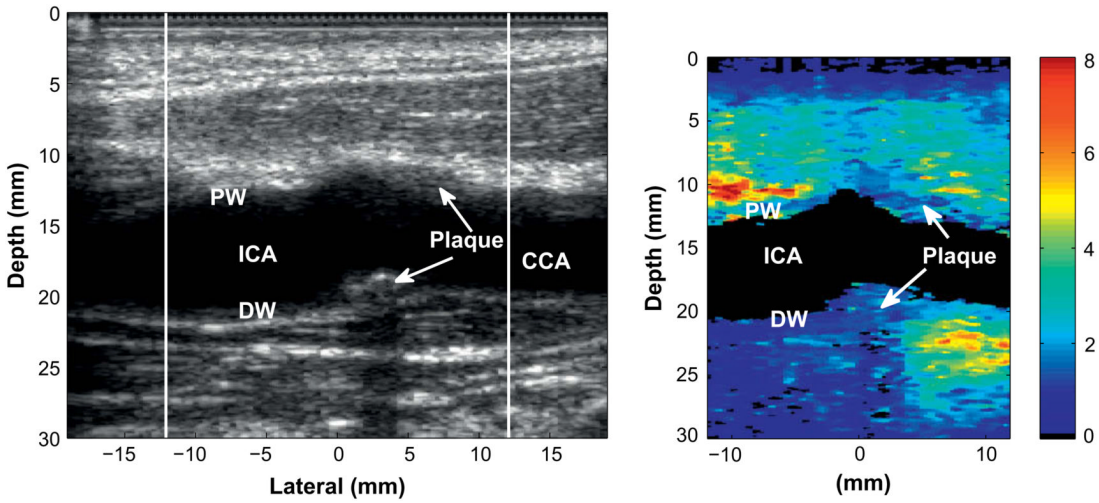

Fig. 4.

Longitudinal view of the plaque shown in Fig. 3. The plaque is visible on the distal wall of the carotid artery and wraps around to the proximal wall. The plaque appears to be heterogeneously stiff.

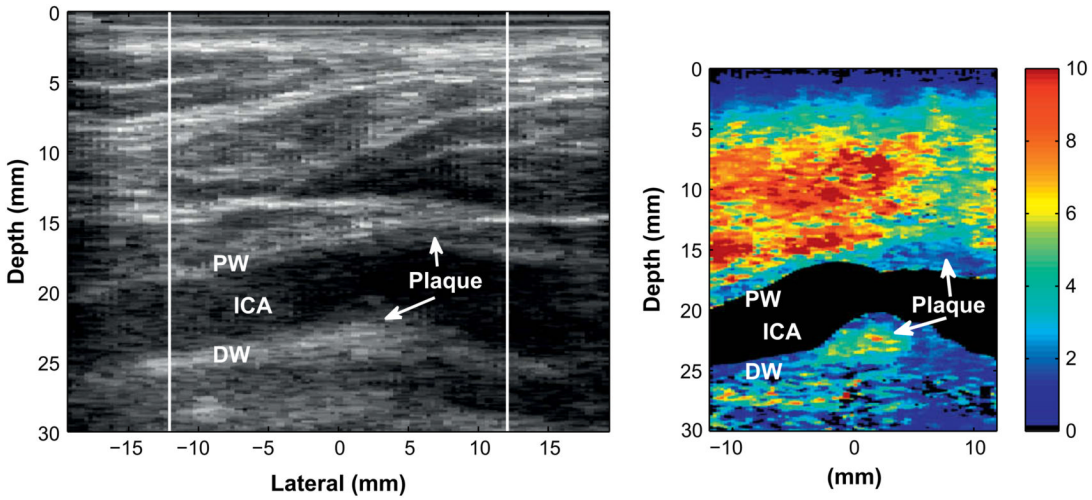

Fig. 5.
Matched B-mode (left) and corresponding ARFI image (right) of a heterogeneous plaque with a compliant region surrounded by a stiff region, indicating a possible soft tissue or lipid pool surrounded by a fibrous cap.

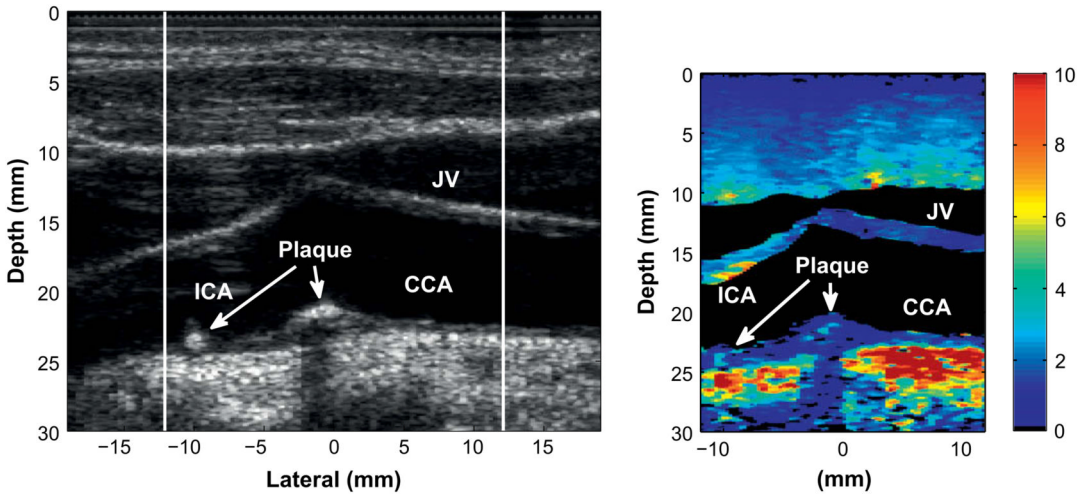

Fig. 6.

Matched B-mode (left) and corresponding ARFI image (right) of a mildly heterogeneous plaque in the carotid bifurcation of an 83-y-old male patient. The plaque contains small, compliant regions in the largest portions of the plaque (indicated by the arrows in the right image, located in the bifurcation and internal carotid artery [ICA]). The size of these regions is approximately 0.5 mm.

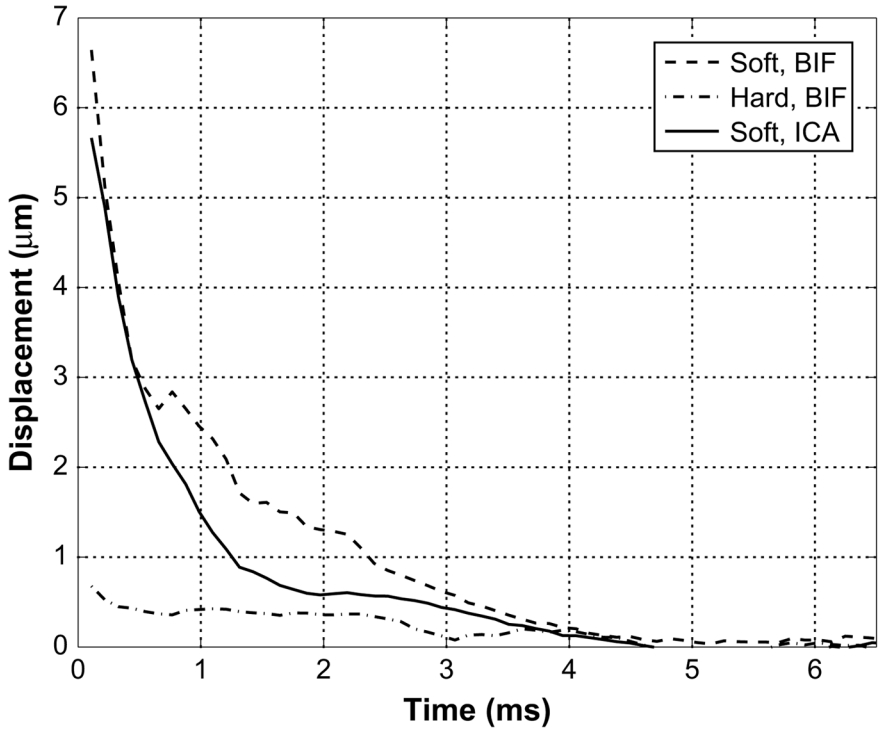

Fig. 7.

The displacements shown over time for the two soft regions located in the bifurcation (BIF) and the internal carotid artery (ICA) and a hard region in the bifurcation in Fig. 6. The soft regions recover to the noise floor in 2.2 and 1.1 ms for the bifurcation and internal carotid regions, respectively and do not displace above the noise floor for the adjacent hard region.

Ultrasound Med Biol. Author manuscript; available in PMC 2010 January 28.

Table 1

Common carotid intima-media thickness from B-mode images, ARIC scores and entire wall thickness from ARFI images for assumed high risk volunteers

Volunteer	Proximal IMT (mm)	Distal IMT (mm)	ARIC (%)	Proximal wall thickness (mm)	Distal wall thickness (mm)
1	0.8	0.7	25	1.0	1.1
2	1.1	0.6	10	1.3	1.4
3	0.5	0.6	30	1.3	0.9
4	1.2	1.1	95	1.9	1.4
5	2.2	1.2	95	2.6	2.5
6	0.8	0.6	15	1.9	2.0
7	N/A	2.1	95	2.5	3.0
8	0.9	0.6	30	1.7	1.4
9	0.8	0.6	10	1.6	1.1
10	0.9	1.0	75	1.4	1.2
11	0.7	1.3	95	1.6	1.6
12	0.9	1.0	90	1.7	1.8
13	0.6	0.5	30	1.4	1.3
14	0.7	0.7	50	1.4	1.7
mean	0.9	0.9	53.2	1.7	1.6
st. dev.	0.4	0.4	35.6	0.4	0.6

ARIC = Atherosclerotic Risk in Communities; ARFI = acoustic radiation force impulse; IMT = intimal-medial thickness.

Table 2

Common carotid intima-media thickness from B-mode images, ARIC scores and entire wall thickness from ARFI images for assumed low risk volunteers

Volunteer	Proximal IMT (mm)	Distal IMT (mm)	ARIC (%)	Proximal wall thickness (mm)	Distal wall thickness (mm)
1	0.6	0.5	N/A	1.2	0.9
2	0.5	0.4	25	1.0	1.0
3	0.6	0.5	10	1.4	1.1
4	0.5	0.5	10	1.6	1.1
5	0.6	0.6	30	1.1	1.1
6	0.6	0.7	50	0.9	1.3
7	0.5	0.5	25	1.3	1.1
8	0.5	0.5	5	1.3	1.1
9	0.5	0.5	25	1.0	1.0
10	0.5	0.5	25	1.3	1.1
mean	0.54	0.5	22.8	1.2	1.1
st. dev.	0.05	0.1	13.5	0.2	0.1

ARIC = Atherosclerotic Risk in Communities; ARFI = acoustic radiation force impulse; IMT = intimal-medial thickness.

Ultrasound Med Biol. Author manuscript; available in PMC 2010 January 28.